crystals

MDPI

Article

Additive Manufacturing of Ceramic-Reinforced Inconel 718: Microstructure and Mechanical Characterization

Yang Qi [1,*], Bo Hu [2], Lei Wang [1], Yanwei Ma [1], Mei Yang [1], Yihang Ma [1] and Pengfei Li [3,*]

[1] School of Mechanical Engineering and Automation, Shenyang Institute of Technology, Shenyang 113122, China
[2] College of Sciences, Shenyang University, Shenyang 110044, China
[3] School of Mechanical Engineering, Jiangsu University, Zhenjiang 212013, China
* Correspondence: 18896662009@163.com (Y.Q.); pengfeili@ujs.edu.cn (P.L.)

Abstract

This study investigates the microstructure and mechanical properties of Inconel 718, a nickel-based alloy, reinforced with ceramic phases via additive manufacturing. Two reinforcement strategies were explored: in situ formation of ceramic phases through titanium powder addition, and direct incorporation of Cr_2O_3 and TiO_2 ceramic particles. Both approaches significantly modified the alloy's microstructure and elemental distribution. The in situ formation method produced leaf-like Ti-rich precipitates (up to 70.13 wt%), while direct ceramic addition suppressed the preferred orientation of the Laves phase and promoted the formation of NbC precipitates. Microhardness increased by 19.4% with titanium addition, compared to a modest 1.3% improvement with direct ceramic addition. Tensile testing revealed that titanium powder enhanced ultimate tensile strength but reduced elongation, whereas direct ceramic addition led to decreases in both strength and ductility. Wear resistance evaluation showed that direct ceramic addition yielded superior performance, evidenced by the lowest friction coefficient (0.514) and smallest wear volume (16,290,782 μm^3). These findings demonstrate the effectiveness of ceramic reinforcement strategies in optimizing the mechanical and tribological behavior of additively manufactured Inconel 718, and offer valuable guidance for the development of wear-resistant components such as those used in hydraulic support systems.

Keywords: ceramic reinforcement; cermet; additive manufacturing; microstructure; mechanical properties

check for updates

Academic Editor: Umberto Prisco

Received: 11 June 2025
Revised: 17 June 2025
Accepted: 19 June 2025
Published: 20 June 2025

Citation: Qi, Y.; Hu, B.; Wang, L.; Ma, Y.; Yang, M.; Ma, Y.; Li, P. Additive Manufacturing of Ceramic-Reinforced Inconel 718: Microstructure and Mechanical Characterization. *Crystals* **2025**, *15*, 585. https://doi.org/10.3390/cryst15070585

Copyright: © 2025 by the authors. Licensee MDPI, Basel, Switzerland. This article is an open access article distributed under the terms and conditions of the Creative Commons Attribution (CC BY) license (https://creativecommons.org/licenses/by/4.0/).

1. Introduction

In the aerospace sector, metal additive manufacturing (AM) is revolutionizing conventional production processes due to its distinct advantages. This technology enables the rapid fabrication of lightweight, high-strength, and high-precision metal components tailored to complex design specifications. Consequently, it significantly shortens development cycles, reduces production costs, and enhances material utilization efficiency [1,2]. Liberated from the limitations of traditional manufacturing techniques, aerospace component design can now achieve more optimized geometries and improved performance characteristics [3,4]. Inconel 718 (IN718), a nickel-based superalloy, is widely used in aerospace applications due to its exceptional combination of having a high strength, excellent high-temperature resistance, corrosion resistance, and good processability, which make it well-suited for demanding service environments. However, to further extend its application scope and service life, improving its wear resistance remains a critical challenge [5,6].

To address this issue, ceramic-reinforced metal matrix composites (MMCs) have emerged as a promising solution. These materials integrate the toughness and ductility of metal matrices with the high hardness, stiffness, and superior wear and thermal resistance of ceramic reinforcements, resulting in significantly enhanced overall performance [7–9]. Such composites not only fulfill the stringent demands of high-performance aerospace materials but also facilitate the fabrication of complex structures through additive manufacturing. This dual advantage has made ceramic-reinforced MMCs a focal point of current research and a key direction for the future development of metal AM technologies in the aerospace industry [10].

The direct incorporation of ceramic particles during additive manufacturing (AM) has been shown to refine microstructures and enhance mechanical properties of metal components [11–13]. Chen et al. [14] used directed energy deposition (DED) to fabricate 15-5PH stainless steels with TiB_2, TiN, TiC, and WC reinforcements. TiB_2 refined martensitic grains, while TiN improved strength and ductility. WC and TiC enhanced both mechanical and corrosion resistance. Hong et al. [15] reinforced Inconel 625 with ultrafine TiC via DED, showing that higher laser energy improved particle refinement and microstructural uniformity. Rojas et al. [16] found that processing parameters notably affected porosity and clad height in WC/NiCrBSi composites. Wang et al. [17] added 5 wt% TiB_2 to a CoCrFeMnNi high-entropy alloy, achieving 99.72% densification and improved fracture resistance. Similarly, Li et al. [18] fabricated TiN-reinforced HEAs via selective laser melting, obtaining ultrafine grains and high wear resistance. Yang et al. [19] incorporated Cr_2O_3 and TiO_2 into 316L stainless steel, improving hardness and wear performance. Shen et al. [20] used spray granulation to produce $Al_2O_3/GdAlO_3$ eutectic ceramics with high microhardness and fracture toughness. Wu et al. [21] reinforced Al_2O_3–ZrO_2 ceramics with TiC particles, reducing cracks and porosity. Qiao et al. [22] reported improved machinability in TiC-reinforced titanium matrix composites due to grain refinement. Overall, these studies confirm that ceramic particle reinforcement during AM can significantly enhance strength, wear resistance, and structural integrity.

Beyond direct ceramic particle addition, high-energy beams such as lasers can induce in situ chemical reactions in the molten pool, forming ceramic reinforcements that improve strength, wear, and corrosion resistance [23–25]. Wei et al. [26] used gas–liquid reactions in laser AM to generate in situ TiC nanoparticles within a titanium matrix, achieving strong interfacial bonding and enhanced strength–ductility balance. Mandal et al. [27] fabricated graphene-reinforced 316 L stainless steel via powder bed fusion, yielding a fully austenitic structure with improved thermal stability and a 6.2% lower thermal expansion coefficient. Riquelme et al. [28] added up to 80 wt% SiC to 316 L steel using laser deposition, observing carbide formation and graphite evolution; hardness peaked then declined with increasing SiC. Traxel et al. [29] developed a Ti/B_4C + BN composite with combined particulate and in situ reinforcements for high-temperature use. Li et al. [30,31] enhanced Inconel 718 and 316 L by adding titanium powder during DED, boosting tensile strength to 911 MPa and microhardness to 629 HV. Hu et al. [32] studied in situ TiB-reinforced titanium composites, revealing a unique petal-like microstructure and correlating reaction energy with density, hardness, and strength. However, in situ synthesis requires precise control of reactants and process conditions, and excessive ceramic formation under rapid solidification may trigger cracking, reducing mechanical performance.

In summary, most existing studies have focused on evaluating the mechanical properties of additively manufactured specimens reinforced by directly added ceramic particles, while limited attention has been given to in situ synthesized ceramic reinforcements. In this study, Inconel 718 nickel-based superalloy was fabricated via additive manufacturing to produce ceramic-reinforced metal matrix composites using two distinct reinforcement

strategies: (1) in situ synthesis of ceramic phases induced by the addition of titanium powder, and (2) direct incorporation of mixed ceramic particles composed of 75 wt% Cr_2O_3 and 25 wt% TiO_2. A comparative investigation was carried out to assess the effectiveness of these two approaches. The analysis encompassed microstructural evolution, phase precipitation behavior, elemental distribution, and key mechanical properties, including microhardness, tensile strength, and wear resistance. Particular attention was given to differences in grain morphology, reinforcement–matrix interfacial bonding, and secondary phase formation, aiming to elucidate the underlying strengthening mechanisms of each strategy. By systematically comparing the two reinforcement approaches, this study seeks to clarify the respective advantages and limitations of in situ synthesized versus ex situ added ceramic phases in enhancing the overall performance of additively manufactured Inconel 718 components. The findings offer valuable insights into the selection of appropriate ceramic reinforcement strategies for high-performance nickel-based superalloy systems processed via additive manufacturing.

2. Experimental Procedure and Methods

The dual-hopper powder feeding system, as illustrated in Figure 1, enabled the simultaneous delivery of IN718 alloy powder and ceramic powder, thereby facilitating the additive manufacturing of heterogeneous material systems. The materials used in this study included IN718 powder, titanium (Ti) powder, and a ceramic powder mixture consisting of 75 wt% Cr_2O_3 and 25 wt% TiO_2. The use of this specific ceramic combination was based on recommendations from the powder manufacturer, who indicated that the mixed powder exhibits excellent resistance to abrasive wear, high-temperature oxidation, and corrosion. All powders had particle size distributions in the range of 53–150 μm. Laser cladding was employed as the additive manufacturing technique, using the following processing parameters: a laser power of 1400 W, total powder feed rate of 1 r/min, scanning speed of 420 mm/min, hatch overlap ratio of 45%, and a layer thickness of 0.7 mm. The sample reinforced with 10 wt% Ti powder was designated as IN718-Ti, while the sample reinforced with 5 wt% of the ceramic powder mixture (75% Cr_2O_3 + 25% TiO_2) was designated as IN718-Ceram.

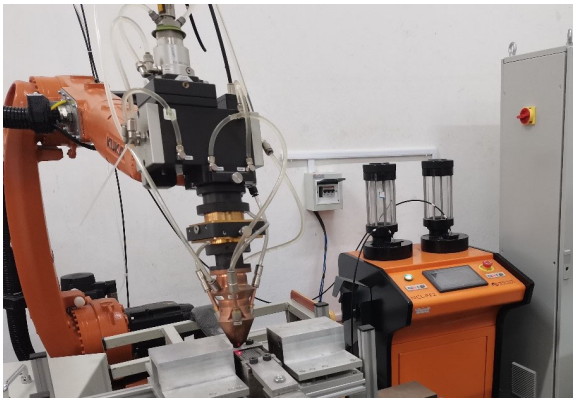


Figure 1. Additive manufacturing device with double material warehouse powder feeding.

For metallographic preparation, the samples were chemically etched in a solution consisting of 10 mL hydrochloric acid (HCl) and 3 mL hydrogen peroxide (H_2O_2) for 10 s. Following etching, the specimens were rinsed with ethanol and dried using compressed air. Microstructural features and elemental distribution were examined using a field-emission scanning electron microscope (FE-SEM) equipped with energy-dispersive X-ray spectroscopy (EDS). Surface wear morphology and wear volume were character-

ized using a Keyence VK-X250K laser confocal microscope (Manufacturer is KEYENCE INTERNATIONAL (BELGIUM) NV/SA, Bedrijvenlaan, Belgium).

3. Results and Discussion

3.1. Microstructure

Figure 2 presents the microstructural morphologies of the additively manufactured IN718 alloy and the two types of ceramic-reinforced composites. In Figure 2a, the unreinforced IN718 sample exhibits distinct short-chain Laves phases with a pronounced orientation, indicating that the thermal gradient during melt pool solidification in the DED process plays a key role in directing phase alignment. In contrast, the microstructure of the IN718-Ti sample (Figure 2b) reveals the formation of leaf-like precipitates resulting from the in situ synthesis of TiO_2 ceramic phases induced by titanium addition. A small number of fine pores are also visible, likely originating from powder feed instability or localized solidification shrinkage. Figure 2c shows the microstructure of the IN718-Ceram sample, reinforced through the direct addition of Cr_2O_3 and TiO_2 ceramic particles. In this case, the Laves phase no longer exhibits preferential orientation, suggesting that the influence of the thermal gradient is mitigated. Instead, the presence of ceramic particles exerts a more significant impact on microstructural evolution and elemental segregation during solidification.

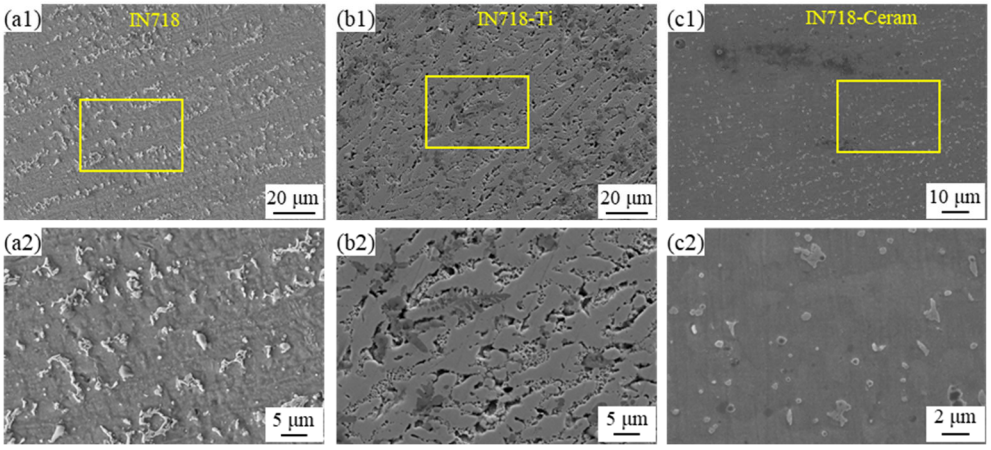


Figure 2. Microstructure of the additively manufactured samples: (**a1**) IN718, (**a2**) IN718 with high magnification, (**b1**) IN718-Ti, (**b2**) IN718-Ti with high magnification, (**c1**) IN718-Ceram, (**c2**) IN718-Ceram with high magnification. The yellow box is the enlarged area.

Figures 3 and 4 present the elemental content and distribution analyses of the additively manufactured IN718 microstructure. Pronounced segregation of the Laves phase is observed, characterized by large, chain-like morphologies. EDS analysis at Spot-2, located within a Laves phase region, reveals a high concentration of niobium (Nb), with a peak content of approximately 27.58 wt%. As typical for a nickel-based alloy, the Ni content remains relatively high in this region. Surrounding the Laves phase are numerous fine, spherical precipitates (Spot-1). EDS results indicate these particles contain a high titanium (Ti) content, reaching up to 27.99 wt%. The concurrent detection of nitrogen (N) and oxygen (O) suggests that these precipitates are likely ceramic phases, possibly titanium oxynitrides. According to the literature, such features are often referred to as "Ring phases," which have been reported to significantly influence the mechanical properties of additively manufactured IN718 alloys [33]. Figure 3 displays the EDS elemental mapping of the scanned area. Nb and molybdenum (Mo) are highly concentrated in the Laves phase regions, confirming their strong partitioning behavior. The co-localization of oxygen further indicates the

susceptibility of the Laves phase to oxidation. Additionally, the fine spherical precipitates show a strong spatial correlation with regions of elevated Ti content, supporting their identification as Ti-rich ceramic particles.

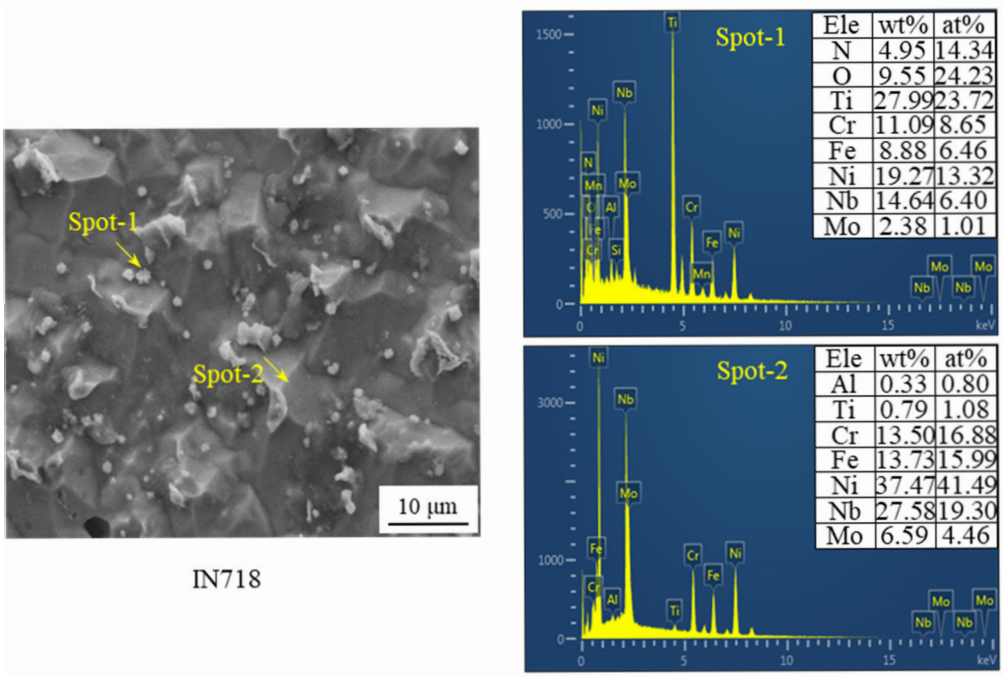


Figure 3. Elemental analysis of precipitates in the microstructure of additively manufactured IN718.

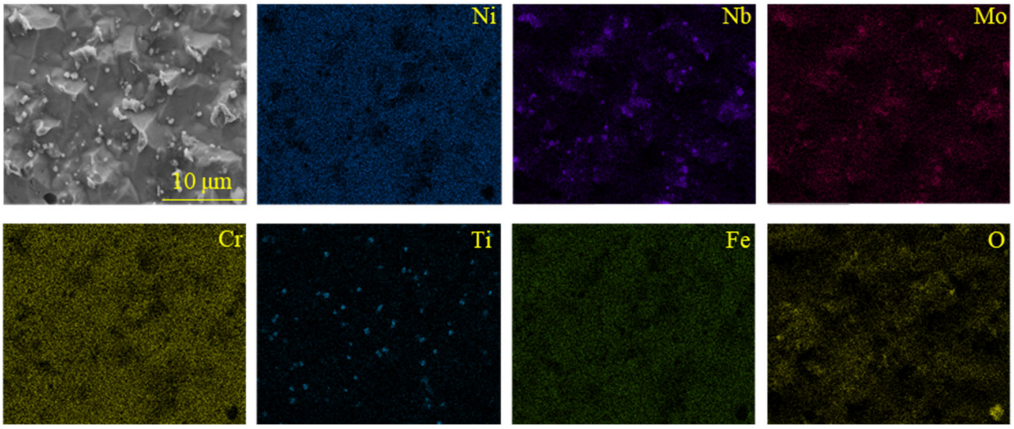


Figure 4. Elemental distribution in the microstructure of additively manufactured IN718.

Figures 5 and 6 present the elemental content and distribution analyses of the additively manufactured IN718 sample reinforced with Ti powder. EDS analysis of the matrix (Spot-3) shows a significant Ti content of 24.53 wt%, alongside substantial amounts of nickel (Ni, 27.09 wt%), iron (Fe, 19.79 wt%), and chromium (Cr, 17.17 wt%), consistent with the primary alloying elements of IN718. This indicates effective dissolution of the added Ti powder into the matrix during the laser cladding process. Analysis of the leaf-like precipitates (Spot-4) reveals a pronounced Ti enrichment, reaching approximately 70.13 wt%, with nitrogen (N) content near 17.05 wt%, confirming that these precipitates are predominantly TiN. The EDS elemental mapping in Figure 6 further validates the high Ti concentration within the leaf-like structures, while the distribution of other elements in the surrounding matrix remains relatively uniform.

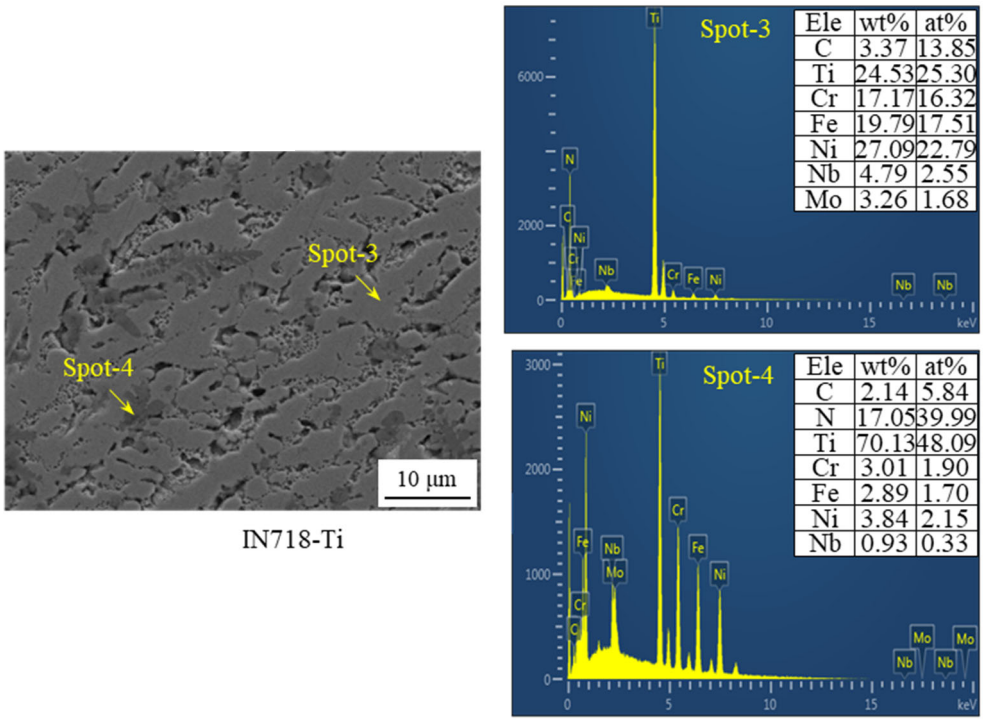


Figure 5. Elemental analysis of precipitates in the microstructure of additively manufactured IN718-Ti.

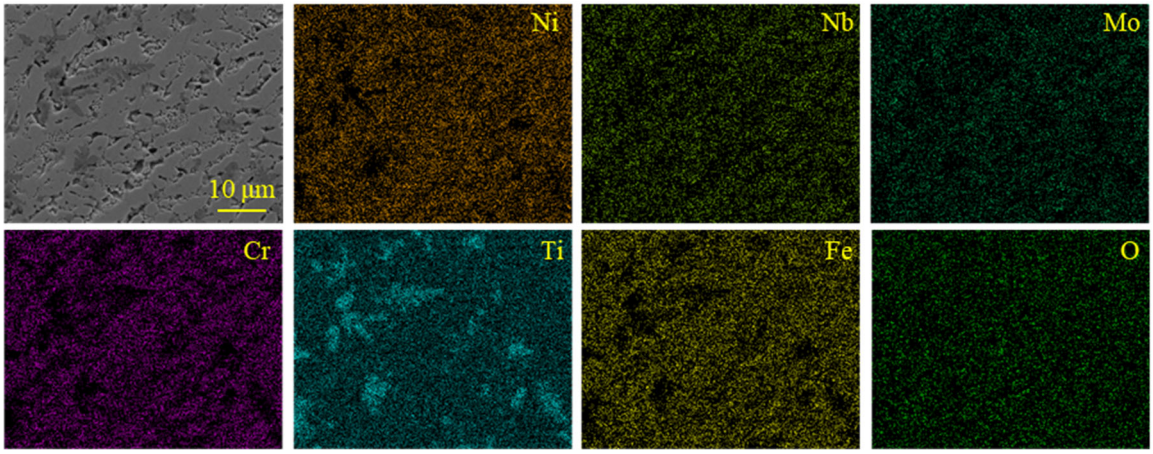


Figure 6. Elemental distribution of the microstructure in additively manufactured IN718-Ti.

Figures 7 and 8 illustrate the elemental content and distribution in the additively manufactured IN718 reinforced with Cr_2O_3 and TiO_2 ceramic particles. EDS analysis of the matrix (Spot-5) shows dominant nickel (Ni) and iron (Fe) content, consistent with the expected composition of IN718. No titanium (Ti) or manganese (Mn) was detected in the matrix. The precipitates formed during the additive manufacturing process exhibit a significant niobium (Nb) content of approximately 25.36 wt%, similar to the Laves phase observed in unreinforced IN718. Notably, these precipitates also contain a high carbon (C) concentration (~21.51 wt%), indicating a substantial presence of NbC carbides. The directly added Cr_2O3 and TiO_2 ceramic particles were not distinctly detected within either the matrix or the precipitates. Elemental mapping in Figure 7 confirms that the precipitates correspond primarily to the Laves phase, enriched in Nb and molybdenum (Mo), with a notable oxygen (O) presence suggesting possible oxidation or oxide formation within these regions.

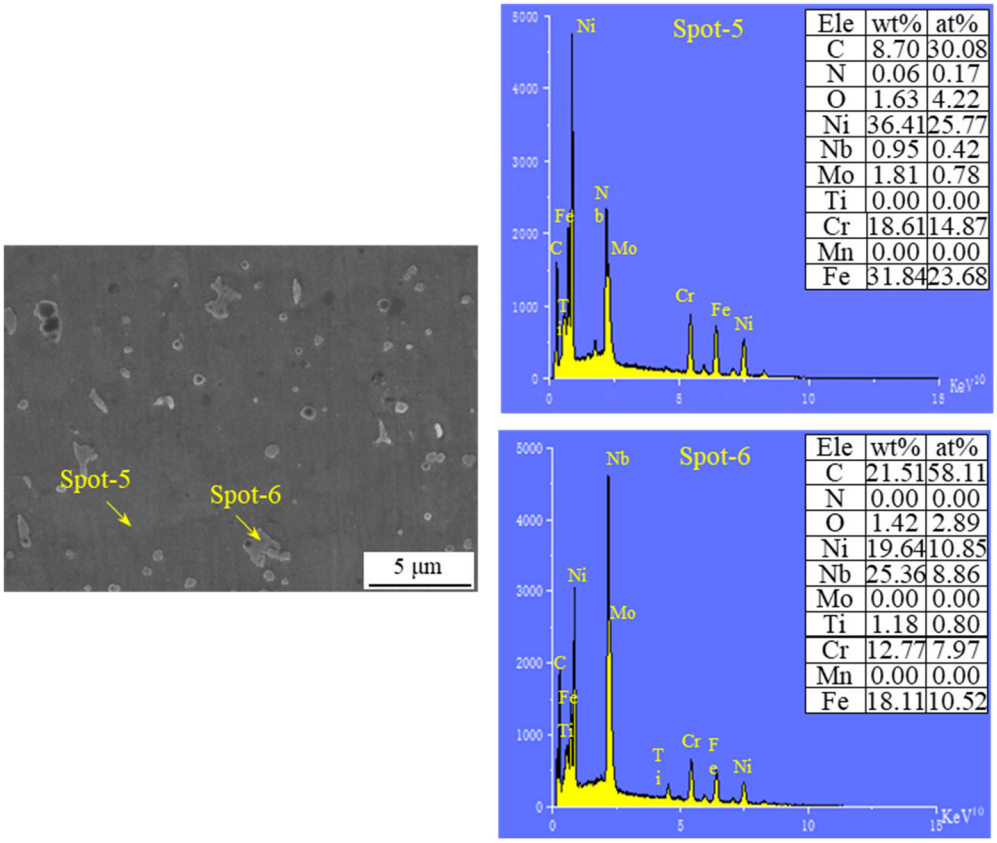


Figure 7. Elemental analysis of precipitates in the microstructure of additively manufactured IN718 with directly added ceramic particles.

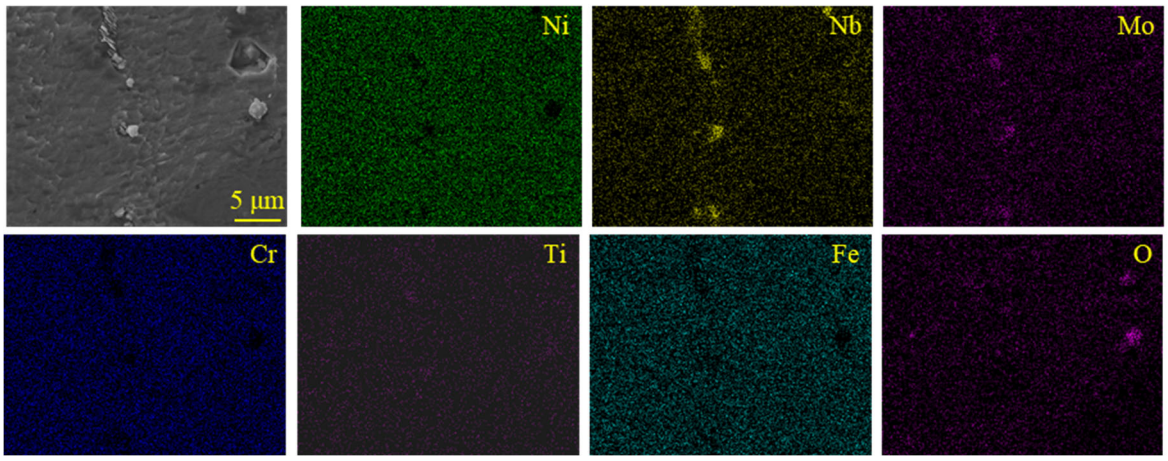


Figure 8. Elemental distribution in the microstructure of additively manufactured IN718 with directly added ceramic particles.

3.2. Microhardness

Figure 9 shows the microhardness results of additively manufactured IN718 with and without ceramic reinforcement. The baseline IN718 exhibited a micro-Vickers hardness of approximately 232 HV. Addition of Ti powder, promoting in situ formation of TiO_2 phases, increased the average hardness to about 277 HV, a notable improvement of 19.4%. In comparison, direct addition of Cr_2O_3 and TiO_2 ceramic particles resulted in a modest hardness increase to approximately 235 HV, only about 1.3% higher than the unreinforced alloy. These results indicate that Ti powder addition significantly enhances the microhardness of IN718, whereas direct ceramic particle addition has minimal effect.

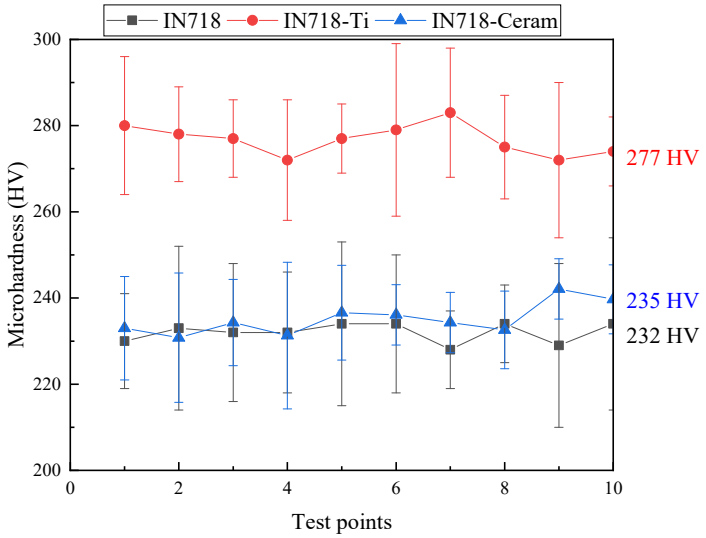


Figure 9. A comparison of microhardness among the three additively manufactured specimens.

3.3. Tensile Properties

Figure 10 and Table 1 present the room-temperature tensile test results of additively manufactured IN718 and samples reinforced with Ti powder or ceramic particles. The unreinforced IN718 showed stable behavior with an elongation of about 16.5%, a yield strength around 513 MPa, and an ultimate tensile strength (UTS) near 779 MPa. The addition of Ti powder increased the average UTS to approximately 797 MPa, but resulted in greater variability, an indistinct yield point, and a significant reduction in elongation to about 5.6%. In contrast, samples with directly added Cr_2O_3 and TiO_2 particles exhibited reduced mechanical properties, with a yield strength near 450 MPa, UTS of roughly 669 MPa, and elongation around 9.9%. Although ceramic additions can enhance certain mechanical aspects, in this study, tensile strength and ductility both decreased. This decline is likely due to weak interfacial bonding between brittle ceramic particles and the metal matrix, which hampers strong chemical or metallurgical bonding. Under tensile stress, ceramic particles are prone to cracking, initiating or propagating microcracks that coalesce into macroscopic fractures, ultimately leading to premature failure [20,21,23].

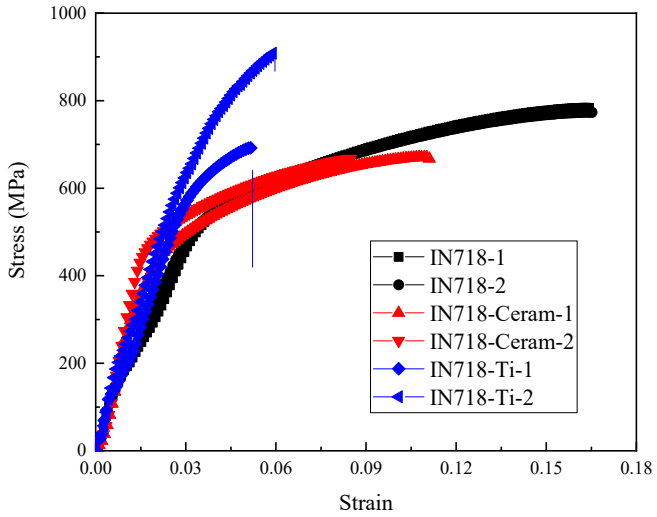


Figure 10. Room-temperature tensile stress–strain curves of the three additively manufactured specimens.

Table 1. Comparison of tensile properties.

	Yield Strength/MPa	Ultimate Tensile Strength/MPa	Elongation
IN718	508 ± 5	784 ± 6	16.5% ± 0.1
IN718-Ceram	423 ± 22	667 ± 30	8.6% ± 1.3
IN718-Ti	/	690 ± 105	5.2% ± 0.4

3.4. Wear Resistance

Figure 11 shows the friction and wear behavior of additively manufactured IN718 before and after the addition of Ti powder and ceramic particles over a 30 min test. The average friction coefficient was calculated during the stable stage near the end. Initially, the friction coefficient rose, then decreased and stabilized within the first 5 min. The unreinforced IN718 exhibited the highest friction coefficient at about 0.719. Adding Ti powder reduced this significantly to approximately 0.633, indicating improved wear resistance. The sample with directly added Cr_2O_3 and TiO_2 ceramic particles showed the lowest friction coefficient, around 0.514. Generally, higher hardness correlates with better wear resistance, which explains the lower friction of the Ti-reinforced sample due to its increased hardness (Figure 9) [34,35]. However, despite minimal hardness improvement, the ceramic particle-reinforced sample had the lowest friction coefficient, likely due to microstructural differences. Notably, the Laves phase size decreased and precipitate morphology changed (Figure 2). Ceramic particles enhance wear resistance by forming a hard protective layer on the metal surface, resisting abrasion and impeding dislocation movement, thereby increasing hardness and deformation resistance.

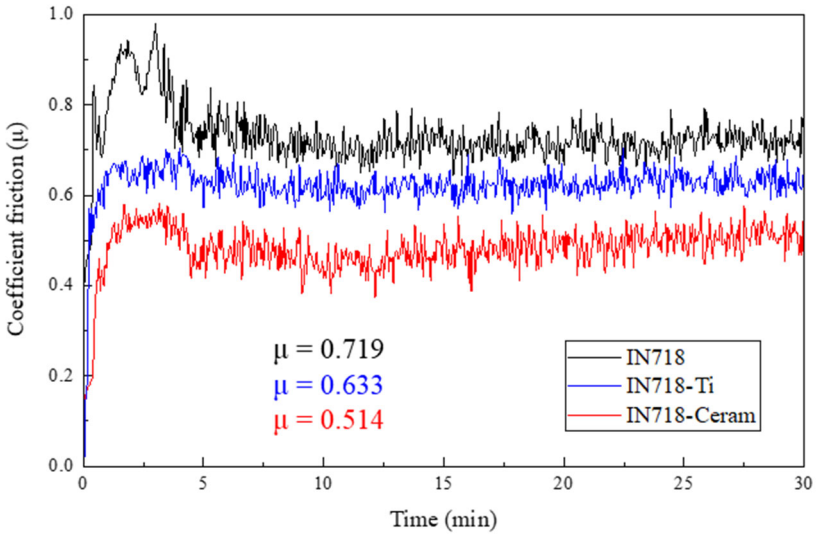


Figure 11. Friction and wear curves of different samples.

Figure 12 shows the 2D and 3D worn morphologies of the samples. The unreinforced IN718 (Figure 12(a1) exhibits clear adhesive wear with indistinct wear track edges. The 3D profile (Figure 12(a2)) reveals that the inner edge rises above the reference plane. The IN718 reinforced with Ti powder shows evident abrasive wear, characterized by deep plowing scratches and no residual surface material (Figure 12(b2)). In contrast, the IN718 with directly added ceramic particles displays unclear inner and outer wear track edges, indicating brittleness. The wear track features significant adhesive wear with substantial flattened block-like debris at the bottom (Figure 12(c1)).

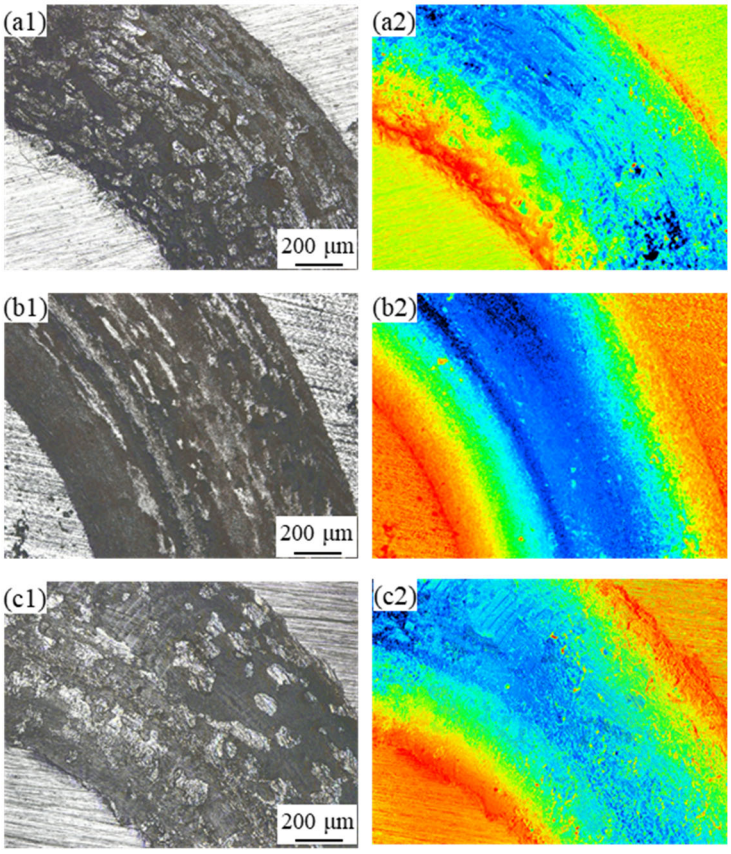


Figure 12. Friction and wear tracks: (**a1**) morphology of IN718, (**a2**) height of IN718, (**b1**) morphology of IN718-Ti, (**b2**) height of IN718-Ti, (**c1**) morphology of IN718-Ceram, (**c2**) height of IN718-Ceram. Red is high, blue is low.

Figure 13 compares the cross-sectional profiles of the wear tracks for the three samples. The wear track of unreinforced IN718 is shallow, with the left edge rising notably above the reference plane (Figure 12(a2)). Its wear track width is about 900 μm, and the depth is around 7 μm. Adding Ti powder increases the wear track width to roughly 1000 μm and the depth to about 25 μm, with a pronounced depression indicating severe plowing wear (Figure 12(b2)). The sample with directly added Cr_2O_3 and TiO_2 shows similar wear width but a slightly smaller depth of approximately 23 μm. These results indicate that both in situ Ti powder reinforcement and direct ceramic particle addition significantly enhance the wear resistance of additively manufactured IN718.

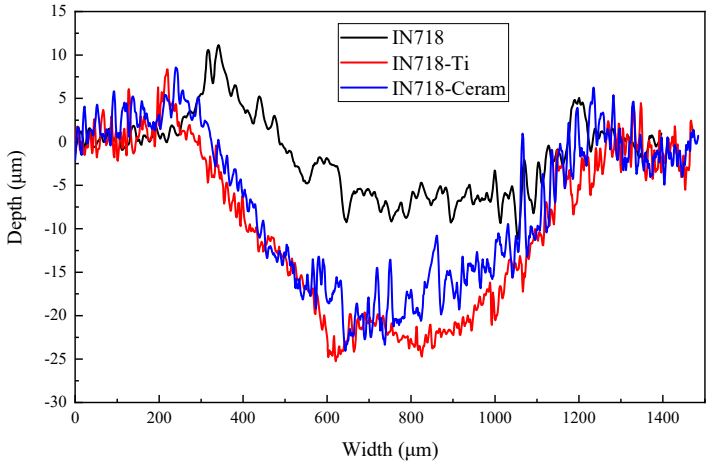
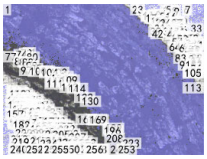
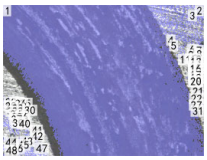
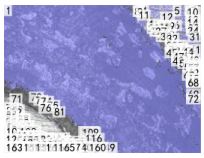


Figure 13. Comparison of friction and wear depth and width.

After the wear tests, the wear volumes of the three samples were measured (Table 2). The IN718 sample showed a much smaller wear volume (6,130,495 μm^3) and area ratio (69.00%) compared to the reinforced samples, mainly due to its shallower wear depth and the significantly elevated inner edge observed in Figure 13, which affected the wear resistance evaluation. Both the Ti powder-added and ceramic particle-added samples exhibited similar total wear volumes, cross-sectional areas, and area ratios, with the Ti-reinforced sample showing slightly higher wear values than the sample with directly added Cr_2O_3 and TiO_2 particles.

Table 2. Comparison of wear volume for different samples.

Samples	Total Worn Volume (μm^3)	Cross-Section Area (μm^2)	Area Ratio (%)	Test Image
IN718	6,130,495	1,049,786	69.00	
IN718-Ti	18,180,621	1,265,710	83.19	
IN718-Ceram	16,290,782	1,220,081	80.23	

4. Conclusions

(1) The addition of ceramic phases during the additive manufacturing process significantly altered the microstructure and elemental distribution of the Inconel 718 nickel-based alloy. The in situ synthesized TiO_2 ceramic phase induced the formation of leaf-like precipitates within the Laves phase, with titanium content reaching approximately 70.13 wt%, indicating TiN as the primary precipitate. Upon direct addition of Cr_2O3 and TiO_2 ceramic particles, the preferred orientation of the Laves phase disappeared, and the precipitates contained about 25.36 wt% Nb and 21.51 wt% C, suggesting the formation of NbC. These microstructural changes directly influenced the mechanical properties of the alloy.

(2) The incorporation of ceramic phases had a pronounced effect on the mechanical properties of Inconel 718. The addition of Ti powder increased the microhardness from 232 HV to 277 HV, corresponding to an improvement of approximately 19.4%. Regarding tensile properties, the ultimate tensile strength rose from 779 MPa to 797 MPa, while the elongation significantly decreased from 16.5% to 5.6%. In contrast, samples with directly added Cr_2O_3 and TiO_2 particles exhibited only a marginal increase in microhardness to 235 HV (1.3% increase), alongside reductions in yield strength and ultimate tensile strength to 450 MPa and 669 MPa, respectively, with an elongation of about 9.9%. In terms of wear resistance, the friction coefficient decreased from 0.719 to 0.633 after Ti powder addition, whereas samples with directly added ceramic particles showed the lowest friction coefficient of 0.514, demonstrating superior wear resistance.

(3) Friction and wear testing revealed that ceramic phase addition markedly enhanced the wear resistance of Inconel 718. The wear volume of the unreinforced sample was 6,130,495 μm^3, with a wear area ratio of 69.00%. Following Ti powder addition, the wear volume increased to 18,180,621 μm^3 and the area ratio to 83.19%. For samples with directly added Cr_2O_3 and TiO_2 particles, the wear volume was 16,290,782 μm^3, with an area ratio of 80.23%. Although the Ti powder-reinforced sample exhibited higher hardness, the directly reinforced ceramic particle samples demonstrated lower friction coefficients and smaller wear volumes, suggesting that microstructural modifications via direct ceramic addition confer significant advantages for optimizing wear resistance.

(4) Both direct ceramic particle addition and in situ ceramic phase synthesis effectively improve the wear resistance of additively manufactured Inconel 718; however, these enhancements come at the expense of reduced tensile properties. The findings of this study provide valuable insights for future research and practical applications, emphasizing the potential of ceramic reinforcement strategies to enhance the wear performance of additively manufactured components.

Author Contributions: Conceptualization, Y.Q., B.H. and P.L.; Methodology, Y.M. (Yanwei Ma), M.Y. and Y.M. (Yihang Ma); Software, Y.Q., B.H., M.Y., Y.M. (Yihang Ma) and P.L.; Validation, Y.Q., B.H., L.W., Y.M. (Yanwei Ma), Y.M. (Yihang Ma) and P.L.; Formal analysis, Y.Q., B.H., L.W., Y.M. (Yanwei Ma) and Y.M. (Yihang Ma); Investigation, B.H., L.W., Y.M. (Yanwei Ma), Y.M. (Yihang Ma) and P.L.; Resources, L.W.; Data curation, L.W.; Writing—original draft, Y.Q. and P.L.; Writing—review & editing, P.L.; Visualization, P.L.; Supervision, Y.M. (Yanwei Ma) and P.L.; Project administration, M.Y.; Funding acquisition, M.Y. All authors have read and agreed to the published version of the manuscript.

Funding: This work was supported by the Liaoning Provincial Natural Science Foundation Joint Fund (2023-MSLH-202) and the State Key Laboratory of Process Engineering Integrated Automation (SAPI-2024-KFKT-05).

Data Availability Statement: The original contributions presented in this study are included in the article. Further inquiries can be directed to the corresponding authors.

Conflicts of Interest: There are no competing interests.

References

1. Kanishka, K.; Acherjee, B. Revolutionizing Manufacturing: A Comprehensive Overview of Additive Manufacturing Processes, Materials, Developments, and Challenges. *J. Manuf. Process.* **2023**, *107*, 574–619. [CrossRef]
2. Chaudhary, R.; Fabbri, P.; Leoni, E.; Mazzanti, F.; Akbari, R.; Antonini, C. Additive Manufacturing by Digital Light Processing: A Review. *Prog. Addit. Manuf.* **2023**, *8*, 331–351. [CrossRef]
3. Chen, H.; Kosiba, K.; Suryanarayana, C.; Lu, T.; Liu, Y.; Wang, Y.; Prashanth, K.G. Feedstock Preparation, Microstructures and Mechanical Properties for Laser-Based Additive Manufacturing of Steel Matrix Composites. *Int. Mater. Rev.* **2023**, *68*, 1192–1244. [CrossRef]
4. Shen, Y.; Wang, L.; Li, L.; Kong, D.; Ma, R.; Liu, L. Microstructure Evolution of 2205 Duplex Stainless Steel (DSS) and Inconel 718 Dissimilar Welded Joints and Impact on Corrosion and Mechanical Behavior. *Mater. Sci. Eng. A* **2025**, *929*, 148136. [CrossRef]
5. Yang, Z.; Wu, G.; Shen, J.; Yin, Y.; Li, L.; Wang, Y.; Tian, Y.; Yao, J. Surface Morphological Characteristics and Mechanisms of Laser-Assisted Electrochemical Polishing on Inconel 718 Alloy. *Opt. Laser Technol.* **2025**, *181*, 111591. [CrossRef]
6. Meng, G.; Gong, Y.; Zhang, J.; Ren, Q.; Zhao, J. Microstructure Effect on the Machinability Behavior of Additive and Conventionally Manufactured Inconel 718 Alloys. *J. Mater. Process. Technol.* **2024**, *324*, 118228. [CrossRef]
7. Kar, A.; Sharma, A.; Kumar, S. A Critical Review on Recent Advancements in Aluminium-Based Metal Matrix Composites. *Crystals* **2024**, *14*, 412. [CrossRef]
8. Li, P. Microstructure and Mechanical Properties of Bimetallic Materials Containing Ceramic Particles Made Using Directed Energy Deposition. *J. Mater. Eng. Perform.* **2024**, *21*, 1–10. [CrossRef]

9. Chen, L.-Y.; Qin, P.; Zhang, L.; Zhang, L.-C. An Overview of Additively Manufactured Metal Matrix Composites: Preparation, Performance, and Challenge. *Int. J. Extrem. Manuf.* **2024**, *6*, 052006. [CrossRef]
10. Karabulut, Y.; Ünal, R. Additive Manufacturing of Ceramic Particle-Reinforced Aluminum-based Metal Matrix Composites: A Review. *J. Mater. Sci.* **2022**, *57*, 19212–19242. [CrossRef]
11. Miao, W.-J.; Wang, S.-Q.; Wang, Z.-H.; Wu, F.-B.; Zhang, Y.-Z.; Ouyang, J.-H.; Wang, Y.-M.; Zou, Y.-C. Additive Manufacturing of Advanced Structural Ceramics for Tribological Applications: Principles, Techniques, Microstructure and Properties. *Lubricants* **2025**, *13*, 112. [CrossRef]
12. Yuan, J.; Zhu, Y.; Wang, J.; Gan, L.; He, M.; Zhang, T.; Li, P.; Qiu, F. Preparation and Application of Mg–Al Composite Oxide/Coconut Shell Carbon Fiber for Effective Removal of Phosphorus from Domestic Sewage. *Food Bioprod. Process.* **2021**, *126*, 293–304. [CrossRef]
13. Yang, Z.; Zhai, X.; Zhang, C.; Shi, J.; Huang, X.; Li, Z.; Zou, X.; Gong, Y.; Holmes, M.; Povey, M. Agar/TiO_2/Radish Anthocyanin/Neem Essential Oil Bionanocomposite Bilayer Films with Improved Bioactive Capability and Electrochemical Writing Property for Banana Preservation. *Food Hydrocoll.* **2022**, *123*, 107187. [CrossRef]
14. Chen, W.; Xu, L.; Zhang, Y.; Han, Y.; Zhao, L.; Jing, H. Additive Manufacturing of High-Performance 15-5PH Stainless Steel Matrix Composites. *Virtual Phys. Prototyp.* **2022**, *17*, 366–381. [CrossRef]
15. Hong, C.; Gu, D.; Dai, D.; Alkhayat, M.; Urban, W.; Yuan, P.; Cao, S.; Gasser, A.; Weisheit, A.; Kelbassa, I.; et al. Laser Additive Manufacturing of Ultrafine TiC Particle Reinforced Inconel 625 Based Composite Parts: Tailored Microstructures and Enhanced Performance. *Mater. Sci. Eng. A* **2015**, *635*, 118–128. [CrossRef]
16. Rojas, J.G.M.; Ghasri-Khouzani, M.; Wolfe, T.; Fleck, B.; Henein, H.; Qureshi, A.J. Preliminary Geometrical and Microstructural Characterization of WC-Reinforced NiCrBSi Matrix Composites Fabricated by Plasma Transferred Arc Additive Manufacturing through Taguchi-Based Experimentation. *Int. J. Adv. Manuf. Technol.* **2021**, *113*, 1451–1468. [CrossRef]
17. Wang, Y.L.; Zhao, L.; Wan, D.; Guan, S.; Chan, K.C. Additive Manufacturing of TiB2-Containing CoCrFeMnNi High-Entropy Alloy Matrix Composites with High Density and Enhanced Mechanical Properties. *Mater. Sci. Eng. A* **2021**, *825*, 141871. [CrossRef]
18. Li, B.; Qian, B.; Xu, Y.; Liu, Z.; Xuan, F. Fine-Structured CoCrFeNiMn High-Entropy Alloy Matrix Composite with 12 wt% TiN Particle Reinforcements via Selective Laser Melting Assisted Additive Manufacturing. *Mater. Lett.* **2019**, *252*, 88–91. [CrossRef]
19. Yang, Q.; Xu, Z.; Li, L.; Li, P. Microstructure and Performance Research on Ceramic-Enhanced Inconel 718 Matrix Composite Using Laser Additive Manufacturing. *Metals* **2023**, *13*, 1525. [CrossRef]
20. Shen, Z.; Su, H.; Liu, Y.; Jiang, H.; Zhao, D.; Guo, Y.; Yu, M.; Zhou, H.; Liu, Y.; Zhang, Z. Laser Additive Manufacturing of Melt-Grown Al_2O_3/$GdAlO_3$ Eutectic Ceramic Composite: Powder Designs and Crack Analysis with Thermo-Mechanical Simulation. *J. Eur. Ceram. Soc.* **2022**, *42*, 6583–6598. [CrossRef]
21. Wu, D.; Yu, X.; Zhao, Z.; Ma, G.; Zhou, C.; Zhang, B.; Ren, G.; Niu, F. One-Step Additive Manufacturing of TiCp Reinforced Al_2O_3–ZrO_2 Eutectic Ceramics Composites by Laser Directed Energy Deposition. *Ceram. Int.* **2023**, *49*, 12758–12771. [CrossRef]
22. Qiao, G.; Zhang, B.; Bai, Q.; Gao, Y.; Du, W.; Zhang, Y. Machinability of TiC-Reinforced Titanium Matrix Composites Fabricated by Additive Manufacturing. *J. Manuf. Process.* **2022**, *76*, 412–418. [CrossRef]
23. Villa, A.; Gianchandani, P.K.; Baino, F. Sustainable Approaches for the Additive Manufacturing of Ceramic Materials. *Ceramics* **2024**, *7*, 291–309. [CrossRef]
24. Luo, L.; Liu, X.; Ma, S.; Li, L.; You, T. Quantification of Zearalenone in Mildewing Cereal Crops Using an Innovative Photoelectrochemical Aptamer Sensing Strategy Based on ZnO-NGQDs Composites. *Food Chem.* **2020**, *322*, 126778. [CrossRef]
25. Ma, S.; Pan, L.G.; You, T.; Wang, K. gC_3N_4/Fe_3O_4 Nanocomposites as Adsorbents Analyzed by UPLC-MS/MS for Highly Sensitive Simultaneous Determination of 27 Mycotoxins in Maize: Aiming at Increasing Purification Efficiency and Reducing Time. *J. Agric. Food Chem.* **2021**, *69*, 4874–4882. [CrossRef] [PubMed]
26. Wei, W.; Zhang, Q.; Wu, W.; Cao, H.; Shen, J.; Fan, S.; Duan, X. Agglomeration-Free Nanoscale TiC Reinforced Titanium Matrix Composites Achieved by in-Situ Laser Additive Manufacturing. *Scr. Mater.* **2020**, *187*, 310–316. [CrossRef]
27. Mandal, A.; Tiwari, J.K.; AlMangour, B.; Das, A.; Sathish, N.; Sharma, R.K.; Rajput, P.; Srivastava, A.K. Microstructural and Thermal Expansion Behaviour of Graphene Reinforced 316L Stainless Steel Matrix Composite Prepared via Powder Bed Fusion Additive Manufacturing. *Results Mater.* **2021**, *11*, 100200. [CrossRef]
28. Riquelme, A.; Sánchez de Rojas Candela, C.; Rodrigo, P.; Rams, J. Influence of Process Parameters in Additive Manufacturing of Highly Reinforced 316L/SiCp Composites. *J. Mater. Process. Technol.* **2022**, *299*, 117325. [CrossRef]
29. Traxel, K.D.; Bandyopadhyay, A. Influence of in Situ Ceramic Reinforcement towards Tailoring Titanium Matrix Composites Using Laser-Based Additive Manufacturing. *Addit. Manuf.* **2020**, *31*, 101004. [CrossRef]
30. Li, P.; Liu, J.; Liu, B.; Li, L.; Zhou, J.; Meng, X.; Lu, J. Microstructure and Mechanical Properties of In-Situ Synthesized Ti (N, C) Strengthen IN718/1040 Steel Laminate by Directed Energy Deposition. *Mater. Sci. Eng. A* **2022**, *846*, 143247. [CrossRef]
31. Li, P.; Yang, Q.; Li, L.; Gong, Y.; Zhou, J.; Lu, J. Microstructure Evolution and Mechanical Properties of in Situ Synthesized Ceramic Reinforced 316L/IN718 Matrix Composites. *J. Manuf. Process.* **2023**, *93*, 214–224. [CrossRef]

32. Hu, Y.; Ning, F.; Wang, X.; Wang, H.; Zhao, B.; Cong, W.; Li, Y. Laser Deposition-Additive Manufacturing of in Situ TiB Reinforced Titanium Matrix Composites: TiB Growth and Part Performance. *Int. J. Adv. Manuf. Technol.* **2017**, *93*, 3409–3418. [CrossRef]
33. Hosseini, E.; Popovich, V.A. A Review of Mechanical Properties of Additively Manufactured Inconel 718. *Addit. Manuf.* **2019**, *30*, 100877. [CrossRef]
34. Jin, B.; Zhang, N.; Yu, H.; Hao, D.; Ma, Y. AlxCoCrFeNiSi High Entropy Alloy Coatings with High Microhardness and Improved Wear Resistance. *Surf. Coatings Technol.* **2020**, *402*, 126328. [CrossRef]
35. Li, Y.; Shi, Y. Microhardness, Wear Resistance, and Corrosion Resistance of AlxCrFeCoNiCu High-Entropy Alloy Coatings on Aluminum by Laser Cladding. *Opt. Laser Technol.* **2021**, *134*, 106632. [CrossRef]

Disclaimer/Publisher's Note: The statements, opinions and data contained in all publications are solely those of the individual author(s) and contributor(s) and not of MDPI and/or the editor(s). MDPI and/or the editor(s) disclaim responsibility for any injury to people or property resulting from any ideas, methods, instructions or products referred to in the content.